View metadata, citation and similar papers at core.ac.uk
brought to you by CORE
provided by Research Archive of Indian Institute of Technology Hyderabad

Optimization of Low-dose Tomography via Binary Sensing Matrices

T. Prasad[1], P.U. Praveen Kumar[1], C.S. Sastry[1], and P.V. Jampana[2]

[1] Department of Mathematics,
Indian Institute of Technology Hyderabad,
Telangana, India
ma13p1004@iith.ac.in, praveen577302@gmail.com, csastry@iith.ac.in

[2] Department of Chemical Engineering,
Indian Institute of Technology Hyderabad,
Telangana, India
pjampana@iith.ac.in

Abstract. X-ray computed tomography (CT) is one of the most widely used imaging modalities for diagnostic tasks in the clinical application. As X-ray dosage given to the patient has potential to induce undesirable clinical consequences, there is a need for reduction in dosage while maintaining good quality in reconstruction. The present work attempts to address low-dose tomography via an optimization method. In particular, we formulate the reconstruction problem in the form of a matrix system involving a binary matrix. We then recover the image deploying the ideas from the emerging field of compressed sensing (CS). Further, we study empirically the radial and angular sampling parameters that result in a binary matrix possessing sparse recovery parameters. The experimental results show that the performance of the proposed binary matrix with reconstruction using TV minimization by Augmented Lagrangian and ALternating direction ALgorithms (TVAL3) gives comparably better results than Wavelet based Orthogonal Matching Pursuit (WOMP) and the Least Squares solution.

Keywords: Discrete Tomography, Compressive Sensing, WOMP, Binary Sensing Matrix, TVAL3

1 Introduction

Computed Tomography (CT) is a technique for reconstructing the cross-section of an object from measurements that are essentially the line integrals of it. The general image reconstruction in CT is a mathematical process that generates an image from X-ray projection data acquired at different angles around the object. As X-rays are harmful to human bodies, the basic objective in CT in medical use is to obtain high quality images from projection data with as little of radiation dosage as possible [11], [19]. This objective was realized in several frameworks ([19], [26] and references therein). There is, however, another dimension to the

CT reconstruction provided by the notion of *sparsity*, which is not yet exploited properly. The emerging theoretical developments, by the name of compressive sensing (CS) have potential in exploiting inherent sparsity in CT images, and resulting in low-dose and stable reconstruction methods.

In the recent CS based CT reconstruction methods [5], [26], the property of CT images being sparse in transform domains such as wavelets, frames was used and reconstruction based on convex optimization was proposed. Unlike the existing methods, the present work, however, aims at analyzing the structure of the underlying matrix. The underlying matrix is binary (with elements being equal to 0 or 1) and we demonstrate empirically that the row restricted matrix satisfies sparse recovery properties. As a result, one may be able to determine the data acquisition geometry (i.e., a particular and restricted set of projection samples) for low-dose reconstruction. We believe that this analysis helps in providing theoretical guarantees for faithful CT image reconstruction.

The current work is an attempt towards giving a handle on the data acquisition geometry for low-dose reconstruction in sparsity framework. The paper is organized as follows: Sections 2, 3 and 4 give an account of related work, brief introductions to CT imaging and basics of the compressive sensing respectively. The proposed reconstruction method via binary sensing matrix is presented in Section 5. The experimental results are discussed in Section 6. Finally, Section 7 gives the concluding remarks.

2 Related Work

In the current literature, CS based techniques are employed to perform CT image reconstruction from incomplete datasets. CS theory allows a sparse signal to be accurately reconstructed from samples far less than what is required by the Shannon/Nyquist sampling theorem [20, 21]. The key to the success of CS is the sparsity of a signal under study. In general, an object is not sparse and often times a sparsifying transform can be used to convert it into a domain in which the signal has a sparse representation. One common sparsifying transform is the discrete gradient transform (DGT) whose coefficients can be summed up to form the so-called total variation (TV).

Inspired by CS theory, various TV minimization algorithms were suggested to solve the few-view, limited-angle, and interior problems. For example, Chen et al. proposed a prior image constrained compressed sensing (PICCS) algorithm for dynamic CT application [6]. Yu and Wang proved that a piecewise constant interior region of interest (ROI) can be uniquely reconstructed by a TV minimizing technique [23, 24]. Xu et al. extended this CS based interior tomography formulation into a Statistical Iterative Reconstruction (SIR) framework [22]. Ritschl et al. proposed an improved TV method within the Adaptive Steepest Descent-Projection Onto Convex Sets (ASD-POCS) framework for clinical applications [18].

As stated already, current work, however, attempts to study the structure of underlying Radon transform matrix and its compliance with the sparse recovery

properties. The study helps one answer the question "what is the data-acquisition geometry such that the sparse recovery properties are satisfied for faithful low-dose reconstruction."

Although these TV-based algorithms are successful in a number of cases, the power of the TV minimization constraint is still limited. First, the TV constraint is a global requirement, which can not directly reflect structures of an object. Second, the DGT operation can not distinguish true structures and image noise. Consequently, images reconstructed with the TV constraint may lose some fine features and generate a blocky appearance in incomplete and noisy cases. In order to overcome the above limitations, in this paper, we employ TV minimization by Augmented Lagrangian and ALternating direction ALgorithms (TVAL3) for reconstruction of tomographic image. This method gives better reconstruction results compared to the state-of-the-art TV minimization methods. We also observe that TVAL3 works well for limited number of rays that are acquired from the CT scanner and the reconstructed image is free from streak artifacts (caused due to scatter) which is generally observed [14] in the reconstructed image using traditional filtered backprojection.

3 Introduction to Computed Tomography

The parallel-beam CT scanning system uses an array of equally spaced unidirectional sources of focused X-ray beams. The basic principle of CT measurement [12] is shown in Fig. 1. The X-ray source, together with primary collimators, provides a fine beam of radiation (ideally an infinitesimally narrow ray) that passes through the object, the intensity of the beam is then measured by a detector. The integral attenuation for each ray position τ is given as:

$$R(\tau) = -\int_{r=0}^{r_p} \mu(\tau, r)dr = \log \frac{I_m}{I_0}, \tag{1}$$

where I_m is the intensity measured by the detector and is dependent on the initial ray intensity I_0 (i.e. $I_m = I_0 \exp(-\int_{r=0}^{r_p} \mu(r)dr)$), and r is the radial distance along the ray from the source at $r = 0$, limited by the radial distance r_p of the projection plane.

The whole measuring arrangement, including the frame enabling the mentioned linear movement, can be rotated as seen in the Fig. 1. This way, we may obtain a projection for any angle θ of the measurement coordinates (τ, r) with respect to the object coordinates (x, y). It is also possible to obtain the projections for a continuum of θ, so that Equation (1) can be rewritten as

$$R(\tau, \theta) = \int_{x_{min}}^{x_{max}} \int_{y_{min}}^{y_{max}} \mu(x, y)\delta(x\cos\theta + y\sin\theta - \tau)dxdy, \tag{2}$$

where the δ-function selects the ray point set, the limits of x and y are given by the object size. Equation (2) is called *Radon transform*, in the continuous-space formulation, obviously, the task of reconstruction of the original image $\mu(x, y)$

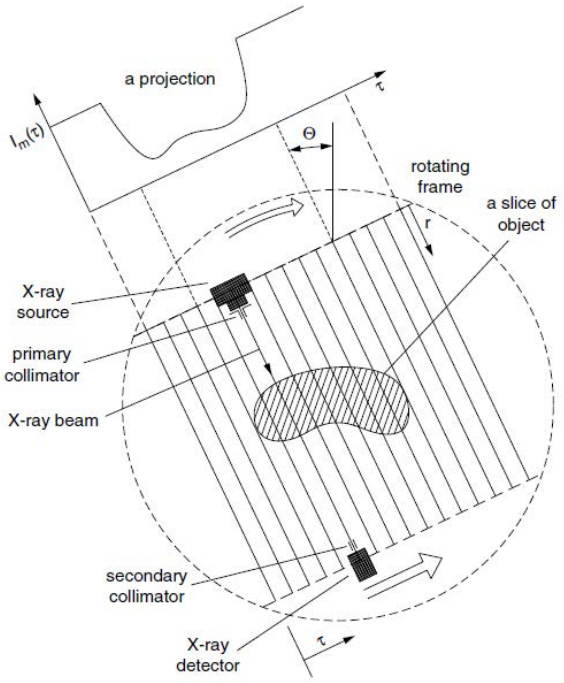

Fig. 1: Principle of measurement of projections basic rectangular arrangement ([12])

from its projection representation $R(\tau, \theta)$ is the problem of finding the inverse Radon transform.

To reconstruct CT image, two major categories of methods exist, namely Analytical Reconstruction and Iterative Reconstruction. Methods based on *Filtered Backprojection* (FBP) are one type of analytical reconstruction. This method is currently used in clinical CT scanners because of its computational efficiency and numerical stability [17]. Despite being computationally expensive, iterative reconstruction methods have potential for low-dose reconstruction [25]. One of the commonly known methods is *Algebraic Reconstruction Technique* (ART) which is iterative in nature. There are different variants of ART [13], viz. Simultaneous Algebraic Reconstruction Technique (SART) [1], Multiplicative Algebraic Reconstruction Technique (MART) [2], etc.

4 Compressive Sensing

Compressed sensing is a signal processing technique for efficiently acquiring and reconstructing a signal, by finding solutions to under-determined linear systems [8]. Consider a full rank matrix $A \in \mathbb{R}^{m \times n}$ with $m < n$ then the linear system

of equations $y = Ax$ where $y \in \mathbb{R}^m$ and $x \in \mathbb{R}^n$ has infinitely many solutions. Among all, the solution with specific property $J(x)$ may be obtained from the following optimization problem:

$$(P_J) : \min_x J(x) \quad \text{subject to } y = Ax.$$

Considering $J(x)$ as $\|x\|_2$, one obtains the following pseudo-inverse solution:

$$\hat{x} = A^\dagger y,$$

where $A^\dagger = A^T(AA^T)^{-1}$. This solution is unique as the function $\|x\|_2$ is strictly convex, and is not in general sparse.

Definition 1. *A vector $x \in \mathbb{R}^n$ is k-sparse if it has k non-zero co-ordinates. i.e., $\|x\|_0 := |\{i|x_i \neq 0\}| = k < n$.*

By considering $J(x)$ as $\|x\|_0$, one may obtain sparse solution from

$$(P_0) : \min_x \|x\|_0 \text{ subject to } y = Ax.$$

The (P_0) problem is a non-convex optimization problem and finding a solution to it is NP-hard. Since (P_0) problem is intractable, several approaches [10] were proposed to approximate (P_0) based on greedy and convex relaxation methods. Among all greedy methods, Orthogonal Matching Pursuit (OMP) is the most popular.

With $\|x\|_1$ in place of $\|x\|_0$, the convex relaxation problem can be posed as

$$(P_1) : \min_x \|x\|_1 \text{ subject to } y = Ax.$$

The $\|\cdot\|_1$ norm in (P_1) tends to provide sparse solution. One way of establishing equivalence between both the problems is through coherence parameter which is defined as follows:

Definition 2. *The mutual coherence μ_A of a matrix A is the largest absolute inner-product between different normalized columns of A. i.e.,*

$$\mu_A = \max_{1 \leq i,j \leq m, i \neq j} \frac{|a_i^T a_j|}{\|a_i\|\|a_j\|}, \text{ where } a_i \text{ is the } i^{th} \text{ column of } A.$$

For any matrix A of order $m \times n$, the mutual coherence is bounded by $\sqrt{\frac{n-m}{m(n-1)}} \leq \mu_A \leq 1$. The lower bound on mutual coherence μ_A is called Welch bound. The following Theorem 1 [9] relates the equivalence between P_0 and P_1 problems via mutual coherence.

Theorem 1. *Let A be an $m \times n$ matrix and let $0 \neq x \in \mathbb{R}^n$ be a solution of (P_0) satisfying*

$$\|x\|_0 < \frac{1}{2}(1 + (\mu(A))^{-1}).$$

Then x is the unique solution of (P_0) and (P_1).

The Restricted Isometry Property (RIP) is another sufficient condition that ensures the equivalence between P_0 and P_1 problems.

Definition 3. *An $m \times n$ matrix A is said to satisfy the Restricted Isometry Property (RIP) of order k with constant $\delta_k \in (0,1)$ if*

$$(1-\delta_k)\|x\|_2^2 \leq \|Ax\|_2^2 \leq (1+\delta_k)\|x\|_2^2 \quad \forall x \in \mathbb{R}^n \ \ with \ \ \|x\|_0 \leq k. \tag{3}$$

Theorem 2. *[4] Suppose an $m \times n$ matrix A satisfies RIP of order $2k$ with constant*

$$\delta_{2k} < \sqrt{2} - 1,$$

then P_0 and P_1 have same k-sparse solution if P_0 has a k-sparse solution.

5 CS in CT: Proposed Method

In this section, we discuss the structure of underlying Radon matrix and an empirical analysis of its compliance with RIP, followed by a convex optimization technique for CT image reconstruction.

5.1 Radon Transform via Binary Matrices

Consider a ray, corresponding to some view θ_i and radial parameter τ_j (Fig. 1). In discrete setting, the Radon measurement may be rewritten as

$$R(\theta_i, \tau_j) = \sum_l I_{i,j}(l) p_l, \tag{4}$$

where $I_{i,j}(l) = \begin{cases} 1 & \text{if } (\theta_i, \tau_j) \text{ ray hits } l^{th} \text{ pixel} \\ 0 & \text{else.} \end{cases}$

In formulating (4), we consider nearest neighbour interpolation of pixels that fall in the path of the ray. The number p_l stands for the pixel value of l^{th} pixel.

The above equation may rewritten as

$$R(\theta_i, \tau_j) = [I_{i,j}(1) \dots I_{i,j}(N)][p_1 \dots p_N]^T, \tag{5}$$

where N is related to the size of the image. For all θ_i and τ_j, proceeding this way, one obtains a matrix system

$$y = Ax, \tag{6}$$

where y contains Radon measurements (i.e. $R(\theta_i, \tau_j)$) in vector form. Accordingly, A is a binary matrix (whose elements are $I_{i,j}(l)$) and x is the vector whose elements p_l. The size of A is dictated by the number of radial and angular sampling parameters and the size of the image to be reconstructed. Suppose A is the matrix corresponding to full set of measurements y, and RA the row restriction of A corresponding to the restricted measurement set Ry (here R may be

treated as a restriction matrix). In low-dose CT, as we deal with a small set of projection samples, the system in (6) becomes under-determined, admitting thereby infinitely many solutions in general. The inherent sparsity present in CT images (as detailed in Table 1) makes CS a natural choice [17] for recovering the underlying image.

Table 1: (%) Measure of natural sparsity in standard Shepp-Logan Phantom image. Here $\|x\|_{0,\epsilon} = |\{i|x_i > \epsilon\}|$ and W represents wavelet transform matrix based on 'db8' [7].

Threshold value (ϵ)	x_ϵ in Spatial domain (i.e. $x_\epsilon = \frac{\|x\|_{0,\epsilon}}{N^2} \times 100$)	$x_{W\epsilon}$ in Wavelet domain (i.e. $x_{W\epsilon} = \frac{\|Wx\|_{0,\epsilon}}{N^2} \times 100$)
10^{-1}	41.68	11.39
10^{-2}	41.82	11.81
10^{-4}	41.82	11.81

5.2 On the RIP Compliance of Radon Matrix

In view of tomographic image possessing natural sparsity, the RIP concept is potentially useful in designing the data acquisition mechanism. This is because the sensing matrix provided by the projection set may be designed so that δ_{2k} is minimized, where k is the expected sparsity of tomographic image, which determines the number of measurements to be used for faithful recovery. As the row restricted binary sensing matrix (RA) is not known to satisfy RIP, we obtain k numerically, such that $\delta_{2k} < \sqrt{2} - 1$ (as in Theorem 2), by looking at the distribution of the quantity:

$$\sigma_k(\alpha) = \|RA\alpha\|_2^2, \text{ for } \alpha \in \mathbb{S}^{n-1}, \ \|\alpha\|_0 \leq k, \tag{7}$$

where $\mathbb{S}^{n-1}$ is unit sphere in $\mathbb{R}^n$. From the values of σ_k, we estimate δ_k as detailed below:

For each k, we considered 1000 vectors, $\alpha \in \mathbb{S}^{n-1}$, such that $\|\alpha\|_0 \leq k$. Here n is related to the size of the image to be reconstructed. From the values of $\sigma_{\{k,\max\}}$ and $\sigma_{\{k,\min\}}$, we estimate δ_k from

$$\delta_k = \max\{1 - \sigma_{\{k,\min\}}, \sigma_{\{k,\max\}} - 1\}. \tag{8}$$

We estimated the values of δ_k for different *sparsity* (k) levels and for four different down-sampling factors (i.e., for different row restriction matrices R generated with uniform distribution). We observed that $k = 21$, $\delta_{2k} < \sqrt{2} - 1$ holds for a matrix of size 2048×4096, 1365×4096, 1024×4096. This observation justifies that the binary sensing matrix provided by the Radon transform appears to possess sparse recovery properties, albeit for low sparsity levels (i.e., k is

small). Though the natural sparsity of CT images (Table 1) does not appear to match the k values obtained by our RIP analysis, however, in simulations it was observed that the reconstruction was of good quality even for lower values of k. Since each row of binary matrix corresponds to a pair of angular and radial parameters, the resulting set of rows provides a kind of handle on the data acquisition geometry for faithful reconstruction. To the best of our knowledge, verifying the RIP-compliance of the matrix of Radon Transform analytically is an open problem.

5.3 Reconstruction via an Optimization Method

Motivated by the empirical analysis connecting sparsity level in image to be reconstructed and the number of measurements needed, one may consider the following optimization technique for recovering x.

$$\min_x \|x\|_{TV}, \text{ subject } to \ y = Ax. \tag{9}$$

where the TV norm of x is defined as

$$\|x\|_{TV} = \|\nabla x\|_1 = \sum_{a,b} \sqrt{(x_{a,b} - x_{a-1,b})^2 + (x_{a,b} - x_{a,b-1})^2}.$$

6 Experimental Results

We carried out experiments to reconstruct the tomographic image (Shepp-Logan) by using binary sensing matrix (measurement matrix) and the measurement vector (projection data). To begin with, we focused on the construction of binary sensing matrix. For constructing it, we considered the following radial and angular sampling [16].

Radial Sampling

$$t_m = \delta_r(p - (n/2)), \tag{10}$$

where $p = \{0, 1, \cdots, n-1\}$, δ_r is the length of detector.

Angular Sampling

$$\theta_l = \frac{q + 0.5}{n}\pi, \tag{11}$$

where $q = \{0, 1, \cdots, n-1\}$. As explained in Section 5, we obtained A with following property:

$$A \in \{0,1\}^{n \times n} \text{ with entries } A_{i,j} = \begin{cases} 1 & \text{for } j \in G_i \\ 0 & \text{for } j \notin G_i \end{cases}$$

the matrix whose entries in the i^{th} row correspond to the detector (sensor) locations for the i^{th} measurement. And $G_i \subset \{1, \cdots, n\}$ corresponds to the set of all detector locations selected for the i-th measurement.

We conducted experiments for R (row restriction matrix) of several sizes, viz. 4096×4096, 2048×4096, 1365×4096 and 1024×4096, obtained as row submatrices of full Radon matrix via uniform distribution (i.e. the corresponding number of measurements are 4096, 2048, 1365 and 1024 respectively). Using solvers viz., WOMP [20], TVAL3 [15] and standard Least Squares, we reconstructed the tomographic image. The algorithms were numerically implemented in the MatLab environment on a machine having 4.0 GB RAM and processor speed of 2.6 GHz. Fig. 2 is the standard Shepp-Logan phantom image which is used for comparison purpose. From Fig. 3, 4 and 5 one can visually observe that TVAL3 gives comparably better reconstruction results than standard Least Squares and WOMP based solvers.

Fig. 2: Standard Shepp-Logan Phantom image.

(a) (b) (c) (d)

Fig. 3: Reconstruction of CT image using Total-Variation Augmented Lagrangian Method with measurement matrix of 4 different sizes: (a) 4096×4096 (b) 2048×4096 (c) 1365×4096 (d) 1024×4096.

In order to evaluate quantitatively the accuracy of reconstruction results, we computed Mean Squared Error (MSE) and Peak Signal to Noise Ratio (PSNR) to measure the similarity between the ground truth and the reconstructed tomographic image. MSE is widely used to evaluate image quality, and is defined

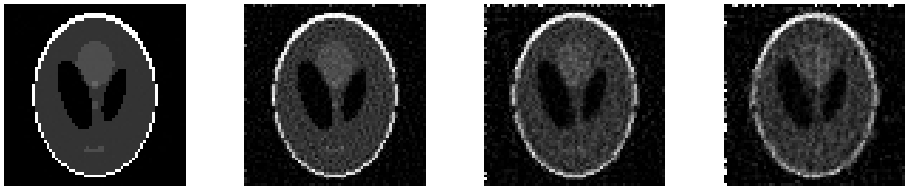

(a) (b) (c) (d)

Fig. 4: Reconstruction of CT image using Least Squares with measurement matrix of 4 different sizes: (a) 4096×4096 (b) 2048×4096 (c) 1365×4096 (d) 1024×4096.

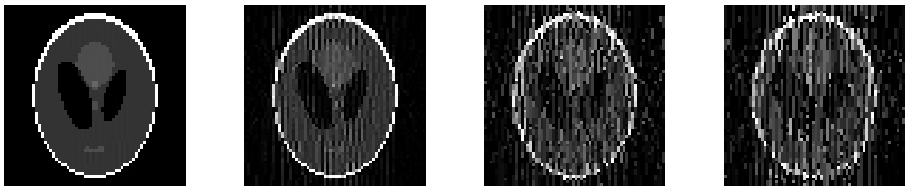

(a) (b) (c) (d)

Fig. 5: Reconstruction of CT image using WOMP with measurement matrix of 4 different sizes: (a) 4096×4096 (b) 2048×4096 (c) 1365×4096 (d) 1024×4096.

as

$$MSE = \frac{\sum_{i=1}^{m} \sum_{j=1}^{n} (x_{i,j} - \widehat{x}_{i,j})^2}{m \times n}, \tag{12}$$

where $x_{i,j}$ is the pixel value of ground truth image and $\widehat{x}_{i,j}$ is the pixel value of reconstructed image.

The corresponding PSNR value is computed as:

$$PSNR = 10 * \log_{10} \frac{(\max(x))^2}{MSE}. \tag{13}$$

Table 2 reports MSE and PSNR errors along with the execution time needed by each of the solvers. The structural similarity (SSIM) index is highly effective way of measuring the structural similarity between two images [21]. Suppose ρ and t are local image patches taken from the same location of two images that are being compared. The local SSIM index measures three similarities of the image patches: the similarity of luminance $l(\rho, t)$, the similarity of contrast $c(\rho, t)$, and the similarity of structures $s(\rho, t)$. The local SSIM [21] is defined as

$$\begin{aligned} S(\rho, t) &= l(\rho, t) \cdot c(\rho, t) \cdot s(\rho, t), \\ S(\rho, t) &= \left(\frac{2\mu_\rho \mu_t + C_1}{\mu_\rho^2 + \mu_t^2 + C_1} \right) \left(\frac{2\sigma_\rho \sigma_t + C_2}{\sigma_\rho^2 + \sigma_t^2 + C_2} \right) \left(\frac{2\sigma_{\rho t} + C_3}{\sigma_\rho \sigma_t + C_3} \right), \end{aligned} \tag{14}$$

Table 2: Performance evaluation of reconstructed tomographic image using solvers viz. TVAL3, Least Squares and WOMP for different dimension of the binary sensing matrix.

Solvers	**Dim. of Binary Sensing Matrix**	**MSE**	**PSNR (dB)**	**SSIM**	**Comp. Time (secs)**
Total Variation	4096 × 4096	8.775e-4	30.57	0.9795	7.5676
Augmented Lagrangian	2048 × 4096	1.977e-3	27.04	0.9552	3.8765
(TVAL3) [15]	1365 × 4096	4.112e-3	23.86	0.9060	2.3527
	1024 × 4096	5.521e-3	22.58	0.8724	1.9151
Least Squares	4096 × 4096	1.677e-6	57.75	0.9997	24.4377
	2048 × 4096	4.607e-3	23.37	0.8634	5.9497
	1365 × 4096	1.458e-2	18.36	0.7732	3.1495
	1024 × 4096	2.245e-2	16.48	0.7028	2.3498
Wavelet based Orthogonal	4096 × 4096	3.545e-6	54.50	0.9995	3364.82
Matching Pursuit(WOMP)	2048 × 4096	0.0068	21.69	0.7830	2234.57
	1365 × 4096	0.0425	13.72	0.4646	565.73
	1024 × 4096	0.0615	12.11	0.3810	167.04

where μ_ρ and μ_t are local means, σ_ρ and σ_t are local standard deviations, and $\sigma_{\rho t}$ is cross-correlation after removing their means. C_1, C_2 and C_3 are stabilizers. The SSIM score of the entire image is then computed by pooling the SSIM map, i.e. by simply averaging the SSIM map. SSIM is highly effective for measuring image quality. Higher SSIM value indicates better image quality.

To better compare the reconstruction results, we plotted the horizontal intensity profile for the chosen row index (here 32^{nd} row was selected). The continuous line corresponds to ground truth image and the dashed line (- - -) corresponds to reconstructed image with different measurement matrices. Fig. 6, 7 and 8 are the line intensity profiles of TVAL3, Least Squares and WOMP respectively.

7 Conclusions

In the present work, we have formulated the problem of reconstruction of low-dose tomography in terms of a matrix system involving a binary matrix. With a view to gaining handle on the data acquisition geometry, we have verified empirically the compliance of the associated binary matrix with sparse recovery properties. Our experimental results have demonstrated that the binary matrix as given by the data acquisition system satisfies RIP for lower sparsity levels. The reconstructions carried out by three different solvers indicate that TVAL3 gives relatively the reconstruction of better quality. The analytical justification of sparse recovery properties of the matrix of Radon transform, nevertheless, is important in proving the efficacy of CS based ideas in CT. Our future efforts shall attempt to address this issue.

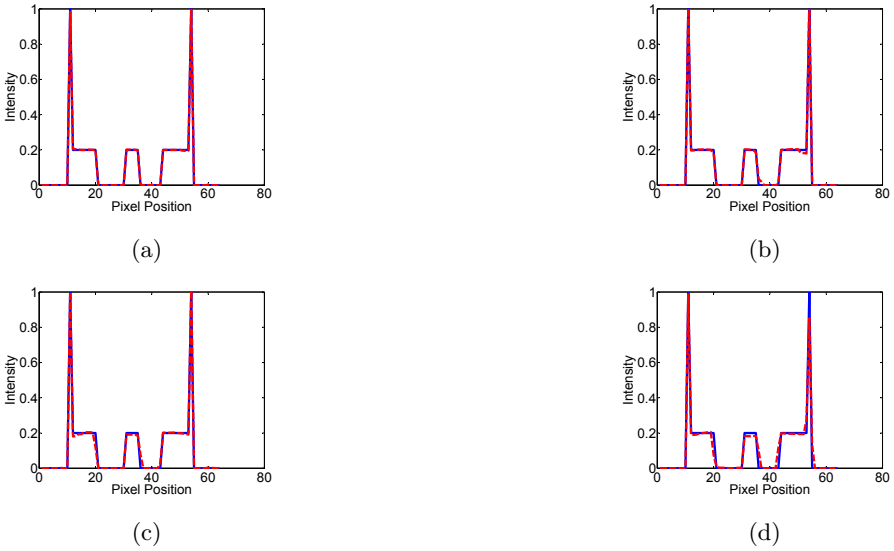

Fig. 6: Comparison of pixel-intensity profiles of ground truth phantom image (continuous line) with reconstructed images (dashed line) using TVAL3 with different dimension of binary sensing matrices: (a) 4096×4096 (b) 2048×4096 (c) 1365×4096 (d) 1024×4096.

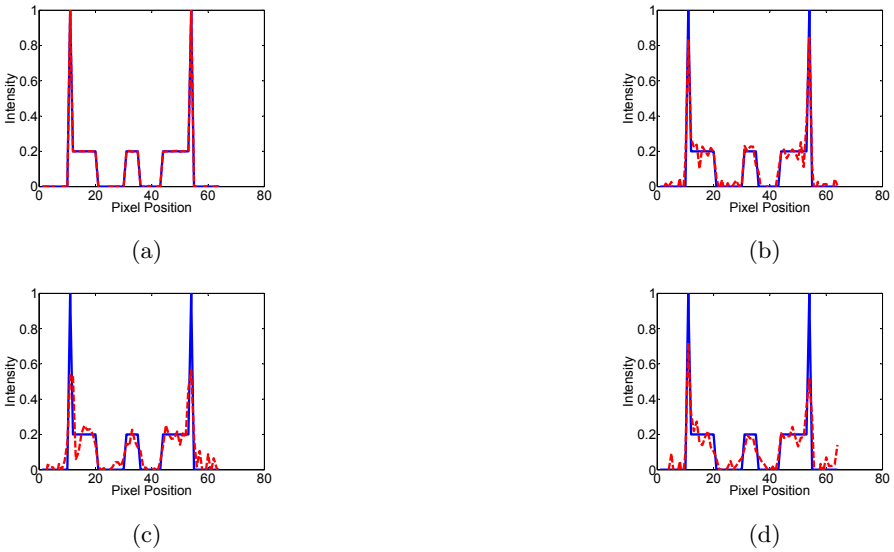

Fig. 7: Comparison of pixel-intensity profiles of ground truth phantom image (continuous line) with reconstructed images (dashed line) using Least Squares with different dimension of binary sensing matrices: (a) 4096×4096 (b) 2048×4096 (c) 1365×4096 (d) 1024×4096.

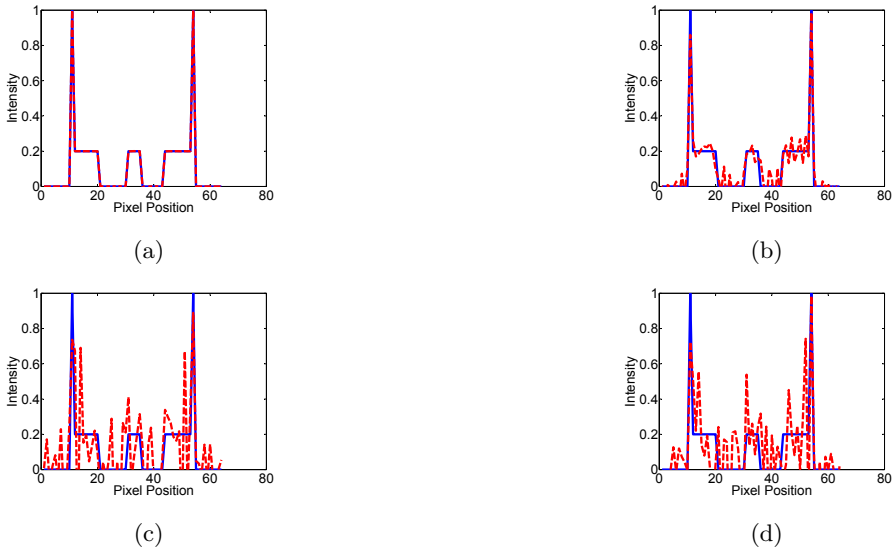

Fig. 8: Comparison of pixel-intensity profiles of ground truth phantom image (continuous line) with reconstructed images (dashed line) using WOMP with different dimension of binary sensing matrices: (a) 4096×4096 (b) 2048×4096 (c) 1365×4096 (d) 1024×4096.

Acknowledgments: One of the authors (CSS) is thankful to CSIR (No. 25(219)/13/EMR-II), Govt. of India, for its support.

A Appendix: Wavelet based Orthogonal Matching Pursuit (WOMP)

The conventional form of orthogonal matching pursuit proposed by Troop et al. [12] is a greedy method which builds up the support set of the reconstructed sparse vector iteratively by adding one index to the current support set at each iteration. The input parameters for the conventional OMP algorithm are the measurement matrix (binary matrix) and the measurement vector. Here, we modified the existing OMP algorithm by incorporating the sparsifying transform (i.e. wavelet transform) to further sparsify the binary matrix. We call the modified algorithm as WOMP, which is given below:

Algorithm

Input Parameters : measurement matrix A, wavelet matrix W, measurement vector b, and the error threshold ϵ_0 **Initialization :** Initialize $k = 0$, and set

- The initial solution $(Wx)^0 = 0$.

- The initial residual $r^0 = b - (AW^T)(Wx)^0 = b$.
- The initial solution support $S^0 = Support\{(Wx)^0\} = \phi$

Main Iteration : Increment k by 1 and perform the following steps:

- ***Sweep***: Compute the errors $\epsilon(j) = \min_{z_j} \|(a_j w_j^T) z_j - r^{k-1}\|_2^2$ for all j using the optimal choice $z_j^* = (a_j^T w_j^T)^T r^{k-1} / \|a_j w_j^T\|_2^2$.
- ***Update Support***: Find a minimizer, j_0 of $\epsilon(j) : \forall j \notin S^{k-1}, \epsilon(j_0) \leqslant \epsilon(j)$, and update $S^k = S^{k-1} \cup \{j_0\}$.
- ***Update Provisional Solution***: Compute $(Wx)^k$, the minimizer of $\|(AW^T)(Wx) - b\|_2^2$ subject to $Support\{(Wx)\} = S^k$
- ***Update Residual***: Compute $r^k = b - (AW^T)(Wx)^k$.
- ***Stopping Rule***: If $\|r^k\|_2 < \epsilon_0$, stop. Otherwise, apply another iteration.

Output: The WOMP solution is $(Wx)^k$ obtained after k iterations.

References

1. Andersen, A.H., Kak, A.C.: Simultaneous algebraic reconstruction technique (SART): A superior implementation of the ART algorithm. Ultrasonic Imaging 6(1), 81–94 (1984)
2. Badea, C., Gordon, R.: Experiments with the nonlinear and chaotic behaviour of the multiplicative algebraic reconstruction technique (MART) algorithm for computed tomography. Physics in Medicine and Biology, 49(8), 1455–1474 (2004)
3. Boyd, S., Vandenberghe, L.: Convex Optimization. Cambridge University Press, New York (2004)
4. Candes, E.J.: The restricted isometry property and its implications for compressed sensing. Comptes Rendus Mathematique, 346, 589–592 (2008)
5. Candes, E.J, Romberg, J.: Practical signal recovery from random projections. Wavelet Applications in Signal and Image Processing XI, Proc. SPIE Conf., 5914 (2005)
6. Chen, G.H., Tang, J., Leng, S.: Prior image constrained compressed sensing (PICCS): A method to accurately reconstruct dynamic CT images from highly undersampled projection data sets. Medical Physics, 35(2), 660–663 (2008)
7. Daubechies, I.: Ten Lectures on Wavelets. Society for Industrial and Applied Mathematics (1992)
8. Donoho, D.L.: Compressed sensing. IEEE Transactions on Information Theory, 52(4), 1289–1306 (2006)
9. Elad, M.: Sparse and Redundant Representations: from Theory to Applications in Signal Processing. Springer (2010)
10. Foucart, S., Rauhut, H.: A Mathematical Introduction to Compressive Sensing. Birkhauser (2013)
11. Frush, D.P., Donnelly, L.F., Rosen, N.S.: Computed tomography and radiation risks: What pediatric health care providers should know. Pediatrics, 112, 951–957 (2003)
12. Jan, J.: Medical Image Processing, Reconstruction and Restoration: Concepts and Methods. CRC Press (2005)
13. Kak, A.C., Slaney, M.: Principles of Computerized Tomographic Imaging. Society for Industrial and Applied Mathematics (2001)

14. Kudo, H., Suzuki, T., Rashed, E.A.: Image reconstruction for sparse-view CT and interior CT – introduction to compressed sensing and differentiated backprojection. Quantitative Imaging in Medicine and Surgery, 3(3), 147–161 (2013)
15. Li, C., Yin, W., Jiang, H., Zhang, Y.: An efficient augmented Lagrangian method with applications to total variation minimization. Computational Optimization and Applications, 56(3), 507–530 (2013)
16. Natterer, F.: The Mathematics of Computerized Tomography, Society for Industrial and Applied Mathematics (2001)
17. Pan, X.C., Sidky, E.Y., Vannier, M.: Why do commercial CT scanners still employ traditional, filtered back-projection for image reconstruction?. Inverse Problems, 25(12), 1230009 (2009)
18. Ritschl, L., Bergner, F., Fleischmann, C., Kachelrieß, M.: Improved total variation-based CT image reconstruction applied to clinical data. Physics in Medicine and Biology, 56(6), 1545–1561 (2011)
19. Sastry, C.S., Das, P.C.: Wavelet based multilevel backprojection algorithm for parallel and fan beam scanning geometries. International Journal of Wavelets, Multiresolution and Information Processing, 4(3), 523–545 (2006)
20. Tropp, J.A., Gilbert, A.C.: Signal recovery from random measurements via orthogonal matching pursuit. IEEE Transactions on Information Theory, 53(12), 4655–4666 (2007)
21. Wang, Z., Bovik, A.C., Sheikh, H.R., Simoncelli, E.P.: Image quality assessment: from error visibility to structural similarity. IEEE Transactions on Image Processing, 13(4), 600–612 (2004)
22. Xu, Q., Mou, X., Wang, G., Sieren, J., Hoffman, E., Yu, H.: Statistical interior tomography. IEEE Transactions on Medical Imaging, 30(5), 1116–1128 (2011)
23. Yu, H.Y., Wang, G.: Compressed sensing based interior tomography. Physics in Medicine and Biology, 54(9), 2791–2805 (2009)
24. Yu, H.Y., Yang, J.S., Jiang, M., Wang, G.: Supplemental analysis on compressed sensing based interior tomography. Physics in Medicine and Biology, 54(18), N425–N432 (2009)
25. Zhang, H., Huang, J., Ma, J., Bian, Z., Feng, Q., Lu, H., Liang, Z., Chen, W.: Iterative reconstruction for X-ray computed tomography using prior-image induced nonlocal regularization. IEEE Transactions on Biomedical Engineering, 61(9), 2367–2378 (2014)
26. Zhou, W., Cai, J.-F., Gao, H.: Adaptive tight frame based medical image reconstruction: a proof-of-concept study for computed tomography. Inverse Problems, 29, 125006 (2013)